Effective gene delivery of *sh*BMP-9 using polyethyleneimine-based core-shell nanoparticles in an animal model of insulin resistance

Yanjun Jia[1#], Dechao Niu[2, 3#], Hong Huang[4], Xinrun Li[1], Kejia Li[1], Ling Li[4], Cheng Zhang[1], Hongting Zheng[5], Zhiming Zhu[6], Yuan Yao[2], XiaoDong Zhao[7], Pei Li[2*], Gangyi Yang[1*]

[1]Department of Endocrinology, the Second Affiliated Hospital, Chongqing Medical University, Chongqing 400010, China

[2]Department of Applied Biology and Chemical Technology, The Hong Kong Polytechnic University, Hung Hom, Kowloon, Hong Kong, China.

[3]Lab of Low-Dimensional Materials Chemistry, School of Materials Science and Engineering, East China University of Science and Technology, Shanghai 200237, China.

[4] Key Laboratory of Diagnostic Medicine (Ministry of Education) and Department of Clinical Biochemistry, College of Laboratory Medicine, Chongqing Medical University, Chongqing, 400016, China

[5]Department of Endocrinology, Xinqiao Hospital, Third Military Medical University, Chongqing 400037, China

[6]Department of Hypertension and Endocrinology, Daping Hospital, Third Military Medical University, Chongqing Institute of Hypertension, Chongqing 400042, China

[7]Chongqing City Key Laboratory of Child Infection and Immunity, Children's Hospital of Chongqing Medical University, Chongqing 400014, China.

[#]**These authors contributed equally to this work.**

[*]**Corresponding authors:** Pei Li, Ph.D.

Department of Applied Biology and Chemical Technology,

The Hong Kong Polytechnic University,

Hung Hom, Kowloon,

Hong Kong, P.R. China.

Tel: + (852)-3400 8721

Fax: + (852)-2364 9932

E-mail: pei.li@polyu.edu.hk

[*]**Co-corresponding authors:** Gangyi Yang, M.D., Ph.D.

Department of Endocrinology,

The Second Affiliated Hospital,

Chongqing Medical University,

74# Linjiang Road, Yuzhong District

Chongqing 400016, China;

Tel: +86-23-68486115

Fax: +86-23-68486115

E-mail: gangyiyang@163.com

Bone morphogenetic protein (BMP)-9 has been reported to associate with insulin resistance and type 2 diabetes mellitus. However, there is still lack of methods to deliver exogenous BMP-9 genes *in vivo* up to now. In this study, we have developed a gene delivery system using polyethyleneimine (PEI)-based core-shell nanoparticles (PCNs) as gene delivery carriers and investigated the effectiveness and safety in delivery of the*sh*BMP-9 gene. The PCNs possessed a well-defined core-shell nanostructure with hydrophobic polymer cores and dense PEI shells. They had uniform particle size with highly positive surface charges. *In vitro* evaluation suggested that the PCNs had high loading capacity of exogenous genes and low cytotoxicity for hepatocytes. The transfection efficiency of PCNs/pENTR-*sh*BMP9 complexes was higher than that of commercial lipofectamine 2000/*sh*BMP9. *In vivo* studies showed that the PCNs/pENTR-shBMP9 transfection led to a significant decrease in hepatic BMP9 expression as compared with pENTR-shBMP9 transfection. Under a HFD feeding, the PCNs/pENTR-shBMP9 mice exhibited aggravated glucose and insulin tolerance. At a molecular level, PCNs/pENTR-shBMP9 mice had a higher level of PEPCK protein and a lower level of InsR and Akt phosphorylation relative to pENTR-shBMP9 mice. These results suggest that the biological effects of PCNs/pENTR-*sh*BMP9 *in vivo* are much more effective than that of pENTR-*sh*BMP9. Therefore, the polyethyleneimine (PEI)-based core-shell nanoparticle can be applied as promising nanocarriers for effective and safe gene delivery.

INTRODUCTION

Type 2 diabetes mellitus (T2DM) represents one of the most common metabolic diseases caused by increasing sedentary lifestyles, obesity, and genetic predisposition. T2DM is characterized by insulin resistance (IR) in peripheral tissues, insulin deficiency, and impaired glucose homeostasis.[1] The pathogenesis of IR is multi-factorial and heterogeneous in origin, involving both genetic and environmental factors. Metabolic derangements associated with IR are due to inadequate insulin action and changes in gene expression in the targeted tissues of insulin, such as liver, muscle, and fat tissues.[2] Therefore, gene therapy through gene modification and delivery to host cells *in vivo* is regarded as a powerful therapeutic method for IR and T2DM.

Bone morphogenetic protein (BMP)-9 is predominantly produced from hepatocytes and intrahepatic biliary epithelial cells, which are a novel member of the transforming growth factor β (TGF-β) superfamily.[3] It was originally identified as chondrogenic and osteogenic factors.[4] Recently, animal studies have demonstrated that BMP-9 has multiple functions including angiogenesis, promoting differentiation of cholinergic neurons in the central nervous system (CNS), and regulating hepatic growth.[5-7] In addition, the BMP-9 has been found to regulate the key enzymes of fatty acid synthesis in the liver, promote insulin release from the pancreas, suppress hepatic glucose production, and increase brown adipogenesis in fat tissue.[8-9] In our recent studies, we found that circulating BMP-9 concentration was significantly lower in newly diagnosed patients with T2DM (nT2DM) than in healthy control. Furthermore, the BMP-9 levels are associated with IR.[10] However, it is unknown at what

concentration of the BMP-9 is sufficient to regulate lipid and glucose metabolism in *vivo*.

Gene therapy has been widely reported to lower blood glucose levels effectively in animal models of T2DM .[11-13] Although both plasmid and viral-based systems have been used to deliver the desired genes *in vivo* and *in vitro*, these delivery systems still suffer from some drawbacks such as low transfection efficacy *in vitro* and short transfection time. In addition, although viral-based gene delivery has an advantage of a rapid onset of the therapeutic effect, it is associated with an increased risk of immunogenicity, chromosomal integration, and inflammatory reaction[14-15]. Therefore, the *in vivo* application of a viral-based gene delivery system still has many limitations due to the issue of *in vivo* safety. Recently, as a typical non-viral gene delivery carrier, branched polyethyleneimine (PEI) polymer has been widely used for gene delivery due to its highly positive charges and excellent complexing ability with the negatively charged plasmids.[16] Moreover, the positive charges of branched PEI can facilitate the endosomal escape of the complexed DNA through a well-established "proton sponge effect" in cells, leading to the successful gene transfection.[17] However, high cytotoxicity and broad particle size distribution of the PEI/DNA complex hampered its applications *in vivo*. To endow the complex with enhanced biocompatible, synthetic or natural polymers such as poly (ethylene glycol) (PEG), poly (L-lactide-co-glycolic acid) (PLGA) and depsipeptide were employed to modify the PEI molecules.[18-20]

Amphiphilic core-shell nanoparticles (NPs) that consist of hydrophobic poly (methyl methacrylate) (PMMA) cores and dense PEI shells have been developed by Li *et al*.[21-22] Potential applications of this type of PEI-based core-shell structured nanoparticles as drug and

gene delivery carriers have been demonstrated *in vitro*.[23-24] Compared to traditional pDNA/PEI complexes gene delivery systems,[25] this type of PEI-based core-shell NPs (PCNs) possess several distinctive advantages: 1) the hairy-like PEI shells provide sufficient concentration and surface area to condense DNA molecules *via* the electrostatic complexation; 2) compared with the pure PEI, the PCNs have much lower cytotoxicity; 3) the obtained DNA/PEI-NP complexes are stable and uniform with high homogeneity. Currently, most studies related to the use of PEI-based gene nanocarriers focus on tumor therapy. Here, we have systematically explored the roles of the PCNs for *in vivo* delivery of *sh*RNA plasmid targeted mouse BMP-9 by observing its metabolic effects.

Materials and Methods

Synthesis of polyethyleneimine-based core-shell nanoparticles (PCNs)

The PCNs were synthesized according to the previous method with a minor modification.[20] Briefly, the branched PEI (25 KDa, 2.0 g) was first completely dissolved in a deionized water, then transferred to a water-jacketed reaction flask equipped with a condenser, a magnetic stirrer and a nitrogen inlet. The mixture was stirred at room temperature under a nitrogen atmosphere for 30 minutes, followed by addition of purified methyl methacrylate (MMA) monomer (8.0 g). An appropriate amount of tert-butyl hydroperoxide (TBHP) (1 mL, 100 mM) was added to the reaction flask. The reaction was allowed at 80 ^{o}C for 2 hr under nitrogen atmosphere. At the end of reaction, the resultant particle dispersion was purified by repeated centrifugation at 15,000 rpm for 30 min and washed with Milli-Q water. Finally, the purified PCNs were dispersed in water or PBS solution for subsequent use.

Characterization of PCNs

Transmission electron microscopy (TEM) image was obtained using a JEOL-100-CXII TEM at an accelerating voltage of 100 kV. The samples were prepared by wetting a carbon-coated copper grid with a small drop of dilute particle dispersion in water (10 μL, 500 ppm). The NPs were stained with diluted phosphotungstic acid (PTA) solution at an appropriate time and then dried at room temperature before TEM analysis. The hydrodynamic diameter and *zeta*-potential of the PEI@PMMA NPs were determined by using a Delsa™ Nano C (Beckman Coulter, Inc., Brea, CA, USA) analyzer with an electrophoretic dynamic light scattering (DLS; a two-laser diode light source with 658 nm wavelength at 30 mW).

The *sh*RNA plasmid targeted mouse BMP-9 (pENTR-*sh*BMP9) and GFP (green fluorescent protein as a marker of transfection)-*sh*RNA vector (pENTR-GFP) were purchased from HANBIO (Shanghai, China). The targeted sequences for *sh*BMP9 were 5'-CAGUACAUGAUCGACUUGU-3'. Recombinant plasmids were confirmed by DNA sequencing (Life Technologies). The absorbance of PCNs-plasmid complexes (PCNs/ pENTR-*sh*BMP9) was analyzed using gel electrophoresis. Plasmid complex was mixed at gradient mass ratios of 20:2, 40:2, 80:2, 120:2, 160:2, and 200:2 (PCNs/ pENTR: *sh*BMP9， μg: μg), then shaken gently on a horizontal shaker for 30 min at 37 ºC, and finally electrophoresed on 1% agarose gels.

Cell culture and cytotoxicity test

HepG2 cells were cultured in a Dulbecco modified Eagle medium (DMEM)

supplemented with 10% fetal bovine serum (Gibco， Invitrogen, Grand Island, NY， USA) at 37 ºC with 5% CO_2. For plasmid transfection, HepG2 cells were plated in 96-well plates at 5 $\times 10^4$ cells / well. Cells were incubated with various gradient concentrations of PCNs (0.5, 1, 2, 3, 4μg/μl) for 12, 24, 48, and 72 h, respectively. Cell viability was measured using a cell counting kit-8 assay (CCK-8, Beyotime, Shanghai, China).

In vitro transfection of HepG2 cells

HepG2 cells were plated in 6-well plates at a density of 5 $\times 10^5$ cells/well and cultured for 12 to 24 h until the cells had completely adhered. Gradient mass ratios (75:1.25, 150:2.5 and 300:5 μg/μg) of PCNs/ pENTR-*sh*BMP9 were added to each well, and the cells were cultured after 12, 24, 48 and 72h, respectively. As a control, HepG2 cells were transfected with 4 μg of the pENTR- *sh*BMP9 plasmid by using 12 μL of Lipofectamine 2000 (Cat: 11668- 019; Invitrogen, Carlsbad, CA, USA) with Opti-MEM I Reduced-serum medium (GIBCO).

***In vivo* study**

Eight-week-old male C57BL/6J mice were purchased from Experimental Animal Centers of Chongqing University of Medical Sciences. Mice were adapted to the environment for 1 week, followed by feeding with either standard diet (SD; 10% calories from fat) or high-fat diet (HFD; 45% of calories from fat; Medicine Inc. Jiangsu, China) for 12 weeks. The mice were randomly divided into 3 groups (6 mice per group). After fasting for 10-12 hours, PCNs, PCNs/ pENTR- *sh*BMP9, or pENTR-*sh*BMP9 was injected into the mice *via* a tail vein at week 11 after receiving the HFD. For intraperitoneal glucose tolerance tests (IGTT)

and insulin tolerance tests (ITT), mice were fasted for 8 hr and injected intraperitoneally with 25% (wt/vol) glucose (2.0 g/kg) or insulin (0.75 U/kg). Blood glucose was measured with the glucose oxidase method before and after injection at specified times. Serum AST and ALT levels were measured with enzymatic colorimetric methods (Roche), and insulin levels were determined with a commercial insulin ELISA kit (Diagnostic Products, Los Angeles, CA, USA). All animal procedures were approved by the Chongqing Medical University Animal Studies Committee and were consistent with the National Institutes of Health guide for the care and use of laboratory animals(NIH Publications No. 8023, revised 1978). Plasma insulin

Real-time quantitative PCR (QRT-PCR) analysis

Total RNA was extracted with a Trizol reagent (Invitrogen, Carlsbad, CA, USA) according to the manufacturer's instructions. Purified RNA was used as the template for first-strand cDNA synthesis using PrimerScript TM RT reagent Kit (Takara Bio Inc. Otsu, Japan). QRT-PCR analysis was performed with a SYBR Premix Ex Taq TMII kit (Takara Bio Inc. Otsu, Japan) and a Corbett Rotor Gene 6000 real-time PCR system (Corbett Research, Sydney, Australia). Relative quantities of mRNA were calculated from CT values using the comparative CT method and normalized with β-actin. The sequences were as follows: sense 5′-TCTTCAACATCTCCATTCCT-3′ and antisense 5′-GGTCTCTGTAGCACTATCC-3′ for human BMP-9; sense 5′- GGAATATGACGCCTATGAGT-3′ and antisense 5′-CTTGTAGA GGATGGAGATGG-3′ for mouse BMP9; sense 5′-AGACCTCTATGCCAACACAGT-3′ and antisense 5′-TCGTACTCCTGCTTGCTGAT-3′ for human β-actin; sense 5′-AAGACCTCT ATGCCAACAC-3′ and antisense 5′-CTGCTTGCTGATCCACAT-3′ for mouse β-actin.

Western blot analysis

Tissues were homogenized and cell lysates were collected. One microliter aliquots of tissue extracts (80 μg) or cell lysates (30 μg) were separated by SDS-polyacrylamide gel electrophoresis and then transferred to poly (vinylidene fluoride) membranes. Immunoblots were blocked in Tris-buffered saline/Tween 20 and 5% skimmed milk or 5% bovine serum albumin for 1 h at room temperature and incubated with primary antibodies including anti-BMP9 (#ab35088; Abcam Inc., Cambridge, UK), anti-PEPCK (#sc-130388; Santa Cruz, Dallas, Texas, USA), anti-phosphor-insulin receptor (p-InsR)(#3026), InsR(#3025), anti-phospho-AKT (#4060; p-AKT,), AKT (#4685; all from Cell Signaling Technology, Boston, MA, USA) and β-actin (#ab8226; Abcam Inc., Cambridge, UK) overnight at 4℃. Following three consecutive 10-min washes, blots were incubated with horseradish peroxidase-conjugated secondary antibody (Santa Cruz, Dallas, Texas, USA) for 1 h at room temperature. The blots were scanned using the Odyssey Infrared Imaging System (LI-COR Biosciences, Lincoln, NE, USA), and quantification of antigen-antibody complexes was performed using analysis software (Bio-Rad, Hercules, CA, USA).

Statistical analysis

Data were presented as means ± SD and analyzed using SPSS20.0 software (Chicago, IL, USA). Statistical significance was determined by one-way ANOVA followed by the Tukey post hoc test or unpaired Student *t*-test. Statistically significant differences were considered at $P < 0.05$.

Results and discussion

Synthesis and characterization of the PEI-based core-shell nanoparticles

The PCNs were synthesized according to the previously published method.[19-20] The morphology of PCNs was characterized with the TEM. **Figure 1a** shows that highly monodispersed spherical nanoparticles were obtained with an average diameter of ~ 280 nm. High-resolution TEM image further revealed that the nanoparticles had well-defined core-shell morphology in a dry state (**Figure 1b**). The dark region in the core represents the PMMA polymer, whereas the light region in the shells represents brush-like PEI component. The thickness of the PEI shell is around 10 nm, and it is homogeneously located on the surface of PMMA core (**Figure 1b**). To further confirm the presence of brush-like PEI shells on the PCNs, the nanoparticles were stained with a diluted phosphotungstic acid (PTA)solution A well defined core-shell nanostructure consisting of PMMA cores (light region) and brush-like PEI shelled (dark region) with a thickness of approximately 100 nm is clearly observed (**Figure 1b insert illustrates**). The darker contrast of the PEI shell is due to a higher electron density region produced by the interaction between the positively charged PEI molecules and negatively charged PTA salt. The colloidal stability and the surface charge of the PEI@PMMA nanoparticle were characterized by dynamic light scattering (DLS) and *zeta*-potential measurement. **Figure 1c** shows that the nanoparticles have an average hydrodynamic diameter of 334 nm in the PBS (pH 7.4), suggesting an excellent stability in biological context. In addition, the *zeta*-potentials of PCNs were pH-dependent at pH 7.4, the PCN nanoparticles have a surface charge of +33.7 mV (**Figure 1d**). The high positive

zeta-potential value at neutral pH was due to the presence of a hairy PEI shell, which is favorable to effectively condense *sh*RNA plasmid with a negative charge and protect them against enzymatic degradation *in vivo*.

The loading capacity of PCNs for pENTR-shBMP9

The *sh*RNA plasmid-loaded PEI@PMMA nanoparticles (denoted as PCNs/shRNA NPs) were obtained through electrostatic interaction between the positively charged PEI shells of the nanoparticles and the negatively charged *sh*RNA plasmid. As shown in **Figure 2a**, when 4μl pENTR-*sh*BMP9 (0.5μg/μl) was combined with 10, 20, 40, 60, 80, and 100μl PCNs (2μg/μl) respectively, the loading capacity increased gradually with increasing PCN concentration. The optimal plasmid loading capacity of PCNs was selected to be 4μl pENTR-*sh*BMP9 (0.5 μg/μl) and 60μl PCNs. In other words, a complete condensation could be achieved with a PCNs/pENTR-*sh*BMP9 mass ratio of 60:1. No redundant plasmid was observed as indicated by the white arrow. Therefore, the loading amount of pENTR-shBMP9 was estimated to be around 16.7 μg/mg.

The cytotoxicity of PCNs in HepG2 cells

The *in vitro* cytotoxicity of the PCNs was evaluated by CCK-8 assays in HepG2 cell lines. Results shown in **Figure 2b** indicate that PCNs have the highest cytotoxic effects in HepG2 cells at 48 h treatment, and then return to baseline at 72 h treatment. Based on these results, it was found that 2 μg/μl concentration of PCNs was a proper concentration for transfection because the rate of cell survival was 97.7 %. Even if the concentration of PCNs was 4 μg/μl,

HepG2 cell survival rates were still higher than 85% (85.0 ± 0.23 %) at 48 h treatment. Additionally, the cytotoxicity of HepG2 cells was also determined at various mass ratios of PCNs to pENTR-shBMP9 (75:1.25, 150:2.5, and 300:5 μg/μg). Results showed that the viability of HepG2 cells was no obvious changes, suggesting that PCNs/pENTR-shBMP9 had low toxicity in HepG2 cells (Supplemental Figure 1).

Biological efficiency of PCNs/ pENTR-shBMP9 transfection in vitro

Transfection efficiency of the PCNs/pENTR-shBMP9 was evaluated in HepG2 cells *in vitro* using a fluorescence microscopy after transfection for at 60 h. The fluorescent image clearly show that PCNs/pENTR-*sh*BMP9 have been translated and expressed into green fluorescent proteins after being delivered into the cytoplasm of HepG2 cells (**Figure 2c**).

To further evaluate the transfection efficiency of the PCNs/ pENTR-*sh*BMP9 in *vitro*, BMP9 mRNA and protein expressions were measured in transfected HepG2 cells using QPCR and western blotting, respectively. HepG2 cells were treated with the PCNs/ pENTR-shBMP9 plasmid at various mass ratios of PCNs to pENTR-shBMP9 (75:1.25, 150:2.5, and 300:5 μg/μg) for 12, 24, 48 and 72h, respectively. Results showed that there were significant inhibitory effects of BMP9 mRNA and protein at the mass ratios of 150:2.5 (μg/μg) (**Figures 3a and b**). The time courses of inhibition effects of PCNs/pENTR-shBMP9 on BMP9 expressions are shown in **Figure 3c-d**. The most significant inhibition of the BMP9 mRNA and protein expression was observed at 48 h after transfection. In addition, the transfection efficiency of the PCNs/pENTR- *sh*BMP9 was compared with lipofectamine 2000/*sh*RNA as a control. It was found that the PCNs/pENTR-shBMP9 induced BMP-9 inhibition in mRNA

and protein levels was more obvious than that of lipofectamine 2000/*sh*RNA in HepG2 cells (Figure **3e-f**). These results suggest that the transfection efficiency of PCNs/pENTR- *sh*BMP9 is higher than that of lipofectamine 2000/*sh*BMP9 in *vitro*.

Biological efficiency of PCNs/pENTR-shBMP9 transfection in vivo

We further evaluated the transfection efficiencies of PCNs/pENTR-shBMP9 in mouse liver tissues. Male C57BL/6J mice were injected with PCNs/pENTR-shBMP9 by a tail vein at gradient mass ratios of 75:1.25, 150:2.5, and 300:5 (μg/μg) for 1h, 1, 3, 5 and 7 day, respectively. Similar to the *in vitro* results, when the mass ratio was 150:2.5 μg/μg (PCNs: pENTR-shBMP9), BMP9 expression in mRNA (**Figure 4a**) and protein (**Figure 4b**) levels in the liver was lower than other mass ratios. In addition, the most significant inhibition of hepatic BMP9 expression was found on day 5 (**Figure 4c-d**).

To compare the transfection efficiencies of PCNs/pENTR-*sh*BMP9 and pENTR -*sh*BMP9 in the liver, mice were injected with PCNs, PCNs/pENTR-*sh*BMP9 or pENTR- *sh*BMP9 by the tail vein. BMP9 expressions in the liver were measured by qPCR and western blotting. The results showed that PCNs/pENTR-shBMP9 treatment led to a significant decrease of hepatic BMP9 expression in both mRNA (~72%) and protein (~35%) levels compare with pENTR-*sh*BMP9 treatment (**Figure 4e-f**). These findings suggest that when the mass ratio (PCNs: pENTR-shBMP9) is 150:2.5 μg/μg, the PCNs/pENTR-shBMP9 gave the highest inhibition rate of BMP9 mRNA and protein expression on day 5 of tail vein injection in mice, and the transfection efficiency of PCNs/ pENTR-shBMP9 is higher than that of pENTR-*sh*BMP9 *in vivo*. Furthermore, treatment mice with PCNs or PCNs/pENTR- *sh*BMP9

have no visible pathological changes in the liver, kidney, and lung, suggesting no obvious cytotoxicity of the PCNs *in vivo* (**Supplemental Figure 2**).

The effects of PCNs/ pENTR-shBMP9 or pENTR-shBMP9 transfer in vivo on glucose metabolism and insulin sensitivity in HFD-fed mice

Efficient gene therapy has been shown to provide new therapeutics for various diseases.[26-28] To further investigate the biological effects of PCNs/pENTR-shBMP9 on glucose metabolism and insulin signaling pathway, HFD-fed C57BL/6J mice, a common IR animal model, were injected with PCNs/pENTR-shBMP9 or pENTR-shBMP9 *via* the tail vein**.** There were no statistical differences in body weight, food intake, serum aspartate aminotransferase (AST), and alanine aminotransferase (ALT) levels in different groups(**Supplemental Table 1**). IGTT and ITT were further performed in these mice to further evaluate insulin sensitivity. Results showed that those mice transfected with the PCNs/pENTR-*sh*BMP9 showed increased fasting blood glucose (FBG) and insulin levels as compared with mice transfected with both pENTR-*sh*BMP9 and PCNs (**Figure 5a and Supplemental Table 1**). During the GTT, PCNs/pENTR-shBMP9 transfer greatly elevated the glucose profile (**Figure 5b**) and the area under the curve for glucose (AUC_{GTT}) (**Figure 5c**) induced by injection of glucose, demonstrating that these mice possessed aggravated glucose tolerance. Accordingly, when compared with pENTR-shBMP9 mice, the PCNs/ pENTR-shBMP9 group during the ITT demonstrated less reduction in their glucose profiles (**Figure 5d**) and the area under the curve for insulin (AUC_{ITT}) (**Figure 5e**) in response to insulin injections. These results suggest that the PCNs/pENTR-*sh*BMP9 treated mice possessed lower insulin sensitivity relative to the

pENTR-*sh*BMP9 mice under HFD feeding. Therefore, the PCNs/ pENTR-*sh*BMP9 transfer has a higher biological efficiency than that of the pENTR-shBMP9, and the BMP9 inhibition exacerbated IR induced by HFD in *vivo*. These results are consistent with our previous study in humans, which demonstrate the relationship between BMP and IR.[29] It is worth mentioned that under a HFD feeding, the PCNs/pENTR-*sh*BMP9 mice showed a higher FBG and further reduced glucose and insulin tolerance relative to with pENTR-*sh*BMP9 mice, indicating a higher biological efficiency of the PCNs/pENTR-*sh*BMP9 *in vivo*.

The effects of PCNs/ pENTR-shBMP9 or pENTR-shBMP9 transfer on insulin signaling pathway in vivo

To further explore the biological efficiency of the PCNs/pENTR-*sh*BMP9 at a molecular level, we first examined the effects of PCNs/pENTR-*sh*BMP9 and pENTR-*sh*BMP9 on PEPCK(Phosphoenolpyruvate Carboxykinase), a key gluconeogenic enzyme, expression in the liver of HFD-fed mice. We found that the expression of PEPCK protein was significantly increased in mice transfected with PCNs/pENTR-*sh*BMP9 when compared with pENTR-*sh*BMP9 transfection (**Figure 5f**). Therefore, our result of *in vivo* study further validated that the PCNs/pENTR- *sh*BMP9 transfection efficiency was much higher than that of general plasmid, and confirmed that BMP9 deficiency increased hepatic gluconeogenesis. Consistent with our previous report,[29] these results further demonstrated that BMP9 may be a regulator of glucose metabolism.

The increase in PEPCK activity and gluconeogenesis in the liver suggests a reduction in insulin sensitivity.[30] Hepatic insulin signaling plays an important role in the regulation of

glucose metabolism *in vivo*.[31] Based on this knowledge, we have investigated the phosphorylation levels of InsR and Akt, two key components in the insulin signaling pathway, in the liver of mice transfected with PCNs/pENTR-*sh*BMP9 or pENTR-*sh*BMP9. Similar to the increase of gluconeogenesis, insulin-stimulated phosphorylation of InsR and Akt in the liver of PCNs/pENTR-*sh*BMP9-transfected mice was reduced by 4-folds and 3.7-folds, respectively, as compared with the controls (a decrease of ~ 62% for InsR and ~69% for Akt) (**Figure 5g-h**), whereas the pENTR-*sh*BMP9 transfection only led to a slight change in the phosphorylation of Akt and InsR in the liver. Therefore, our studies have validated this gene transfer system by showing its ability to regulate the insulin signaling molecule *in vivo* to control glucose metabolism and IR. Therefore, these results further confirm that the biological effects of PCNs/pENTR-*sh*BMP9 *in vivo* are stronger than that of the pENTR-*sh*BMP9.

Conclusions

Here, we have systematically evaluated the *in vitro* and *in vivo* gene delivery ability of PCNs/pENTR-shBMP9 for IR. The as-prepared PCNs possessed a well-defined core-shell nanostructure, relative narrow size distribution, highly positive charges, strong adsorption ability, high capacity for loading with exogenous genes, and low cytotoxicity. Our results revealed that the present PCNs-mediated gene delivery system is effective and safe in transporting and delivering genes. This nanotechnology-based modality can be developed as a new therapeutic strategy for IR individuals and T2DM patients without any apparent toxicity for both *in vivo and in vitro* gene deliveries.

Acknowledgments

This work was supported by grants from National Natural Science Foundation (No.81500666, 81270913, 81470045, and 81570752), the Natural Science Foundation Project of CQ (No. cstc2015jcyjA10084 and cstc2013jcyjA10067) and the Science and Technology Key Program of Health Bureau of Chongqing (2015ZDXM038).

Conflict of Interests Disclosure

No potential conflicts of interest relevant to this article were reported.

Notes and references

1 Meier JJ, Nauck MA, Nat Clin Pract Endocrinol Metab., 2008, **4**, 606-607.

2 Jean M, Alameh M, Buschmann M.D and Merzouki A, Gene Ther., 2011, **18**, 807-816.

3 Miller AF, Harvey SA, Thies RS and Olson MS, J Biol Chem., 2000, **275**, 17937-17945.

4 Sharff KA, Song WX, Luo X, Tang N, Luo J, Chen J, Bi Y, He BC, Huang J, Li X, Jiang W, Zhu GH, Su Y, He Y, Shen J, Wang Y, Chen L, Zuo GW, Liu B, Pan X, Reid RR, Luu HH, Haydon RC and He TC, J Biol Chem., 2009, **284**, 649-659.

5 David L, Feige JJ and Bailly S, Cytokine Growth Factor Rev., 2009, **20**, 203-212.

6 Lopez-Coviella I, Berse B, Krauss R, Thies RS and Blusztajn JK, Science., 2000, **289**, 313–316.

7 Song JJ, Celeste AJ, Kong FM, Jirtle RL, Rosen V and Thies RS, Endocrinology., 1996, **136**, 4293–4297.

8 Chen C, Grzegorzewski KJ, Barash S, Zhao Q, Schneider H, Wang Q, Singh M, Pukac L,

Bell AC, Duan R, Coleman T, Duttaroy A, Cheng S, Hirsch J, Zhang L，Lazard Y，Fischer C， Barber MC， Ma ZD， Zhang YQ， Reavey P， Zhong L, Teng B, Sanyal I, Ruben SM, Blondel O and Birse CE, Nat Biotechnol., 2003, **21**, 294-301.

9 Kuo MM, Kim S, Tseng CY, Jeon YH, Choe S and Lee DK, Biomaterials., 2014, **35**, 3172-3179.

10 Luo Y, Li L, Xu X, Wu T, Yang M, Zhang C, Mou H, Zhou T, Jia Y, Cai C, Liu H, Yang G and Zhang X, Clin Sci (Lond)., 2017, **131**, 239-246.

11 Alexander IE, Cunningham SC, Logan GJ and Christodoulou J, Gene Ther., 2008, **15**, 831-839.

12 Jean M, Alameh M, Buschmann MD and Merzouki A, Gene Ther., 2011, **18**, 807–816.

13 Lee YH, Kim JS, Kim JE, Lee MH, Jeon JG, Park IS and Yi HK, Nanomedicine., 2017, **13**,1821-1832.

14 Robbins PD, Ghivizzani SC, Pharmacol Ther., 1998, **80**, 35-47.

15 Petrs-Silva H, Linden R, Curr Gene Ther., 2013, **13**, 335-345.

16 Wang X, Niu D, Hu C and Li P, Curr Pharm Des., 2015, **21**, 6140-6156.

17 Nel AE, Mädler L, Velegol D, Xia T, Hoek EM, Somasundaran P, Klaessig F, Castranova V and Thompson M, Nat Mater., 2009, **8**, 543-557.

18 Petersen H, Fechner PM, Martin AL, Kunath K, Stolnik S, Roberts CJ, Fischer D, Davies MC and Kissel T, Bioconjug Chem., 2002, **13**, 845-854.

19 Lee MS, Kim MG, Jang YL, Lee K, Kim TG, Kim SH, Park TG, Kim HT and Jeong JH, Macromolecular Res., 2011, **19**, 688-693.

20 Li Q, Shi C, Zhang W, Behl M, Lendlein A and Feng Y, Adv Healthc Mater., 2015, **4**,

1225-1235.

21 Li P, Zhu JM, Sunintaboon P, and Harris FW, Langmuir., 2002, **18**, 8641-8646.

22 Li W, Li P, Macromol Rapid Commun., 2010, **28**, 2267-2271.

23 Zhu J, Tang A, Law LP, Feng M, Ho KM, Lee DK, Harris FW and Li P, Bioconjug Chem., 2005, **16**, 139-146.

24 Siu YS, Li L, Leung MF, Lee KL and Li P, Biointerphases., 2012, **7**, 16.

25 Midoux P, Breuzard G, Gomez JP and Pichon C, Curr Gene Ther., 2008, **8**, 335-352.

26 Liu J, Song L, Liu S, Jiang Q, Liu Q, Li N, Wang ZG and Ding B, Nano Lett., 2018, **18**, 3328-3334.

27 Sun S, Xu Y, Fu P, Chen M, Sun S, Zhao R, Wang J, Liang X and Wang S, **Nanoscale**., 2018,**10**,19945-19956.

28 Guan J, Sun J, Sun F, Lou B, Zhang D, Mashayekhi V, Sadeghi N, Storm G, Mastrobattista E and He Z, Nanoscale., 2017 , **9**, 9190-9201.

29 Xu XH, Li XQ, Yang GY, Li L, Hu WJ, Zhang LL, Liu H, Zheng HT, Tan MH and Zhu DP, Sci Rep., 2017, **7**, 17529.

30 Luo XH, Li K, Zhang C, Yang GY, Yang ML, Jia YJ, Zhang LL, Ma ZA, Boden G and Li L, Int J Obes (Lond)., 2016, **40**, 947-954.

31 Yang ML, Zhang ZH, Wang C, Li K, Li SB, Boden G, Li L and Yang GY , Diabetes., 2012, **61**, 1959-1968.

Figure 1

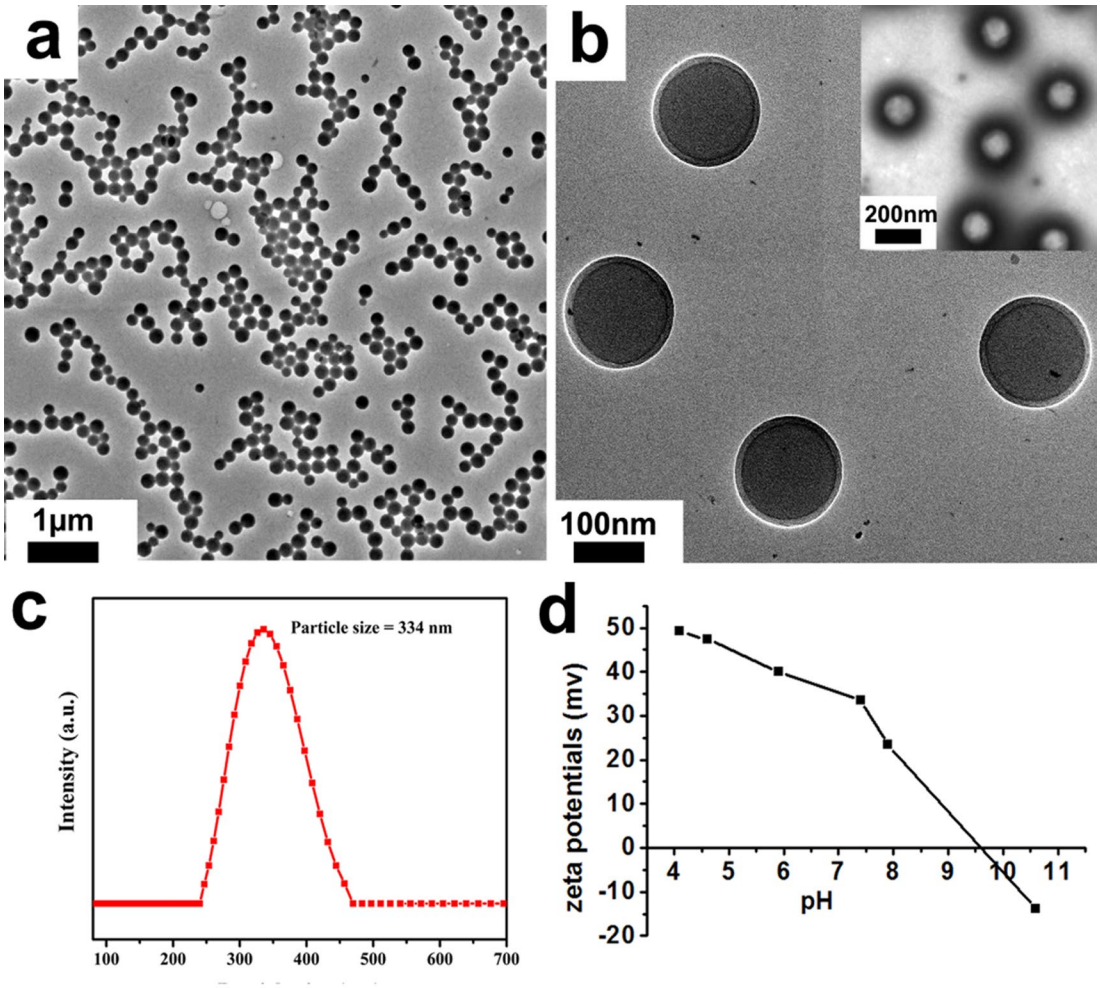

Figure 1. Morphology of the PCNs. **(a-b)** TEM image (Illustrations of **b**: High-revolution TEM image of the PCNs, which was stained with 0.5% w/w phosphotungstic acid solution for 1 min). **(c)** Hydrodynamic diameter of the PCNs in PBS buffer solution. **(d)** PH-dependence of the ζ-potentials of the PEI@PMMA nanoparticles.

Figure 2

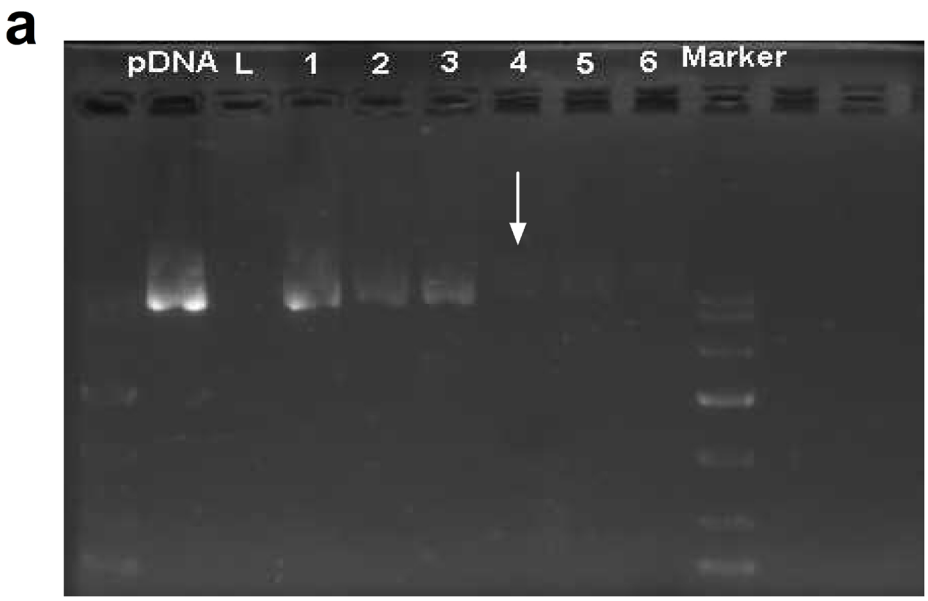
a
pDNA
L
1
2
3
4
5
6
Marker

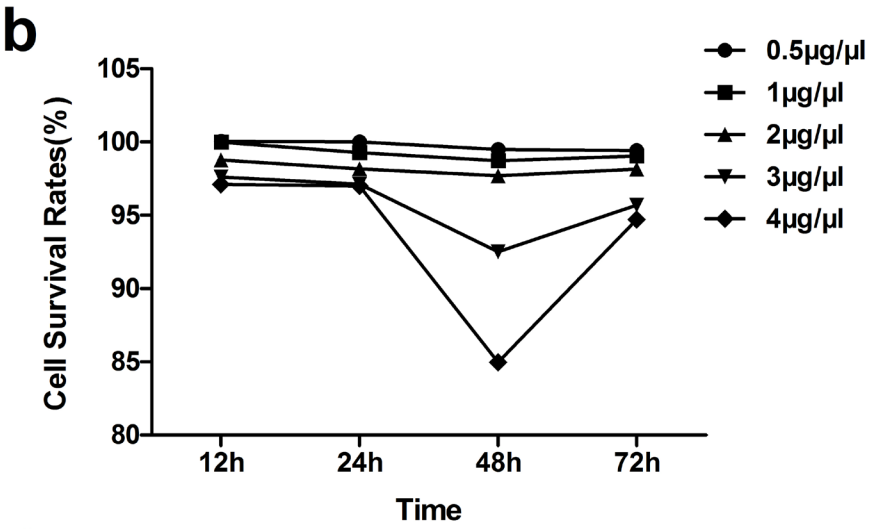
b
Cell Survival Rates(%)
105
100
95
90
85
80
12h
24h
48h
72h
Time
0.5μg/μl
1μg/μl
2μg/μl
3μg/μl
4μg/μl

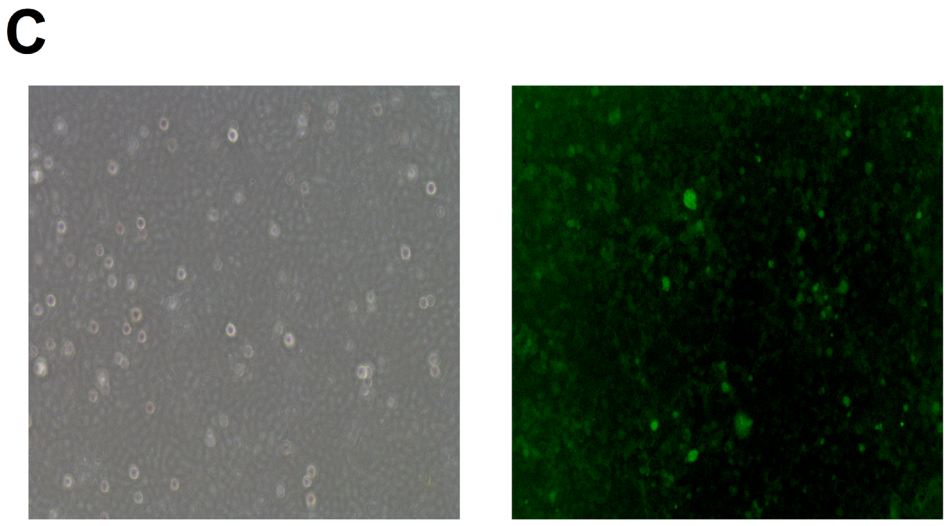
C

Figure 2. The gene loading capacity and cytotoxicity of the PCNs. **(a)** The PCNs-plasmid complexes (PCNs/pENTR-*sh*BMP9) were mixed at gradient mass ratios of 20:2, 40:2, 80:2, 120:2, 160:2, 200:2 (μg: μg, orderly represented by 1, 2, 3, 4, 5 and 6, respectively; loading marker denoted as M), and finally electrophoresed on 1% agarose gels. The adsorption showed by gel electrophoresis was close to 100%, when the PCNs/ pENTR-shBMP9 mass ratio reached 60:1. **(b)** CCK-8 assays indicated the cytotoxic effects of PCNs in HepG2 cells. **(c)** The fluorescent image (100×) of HepG2 cells expressing GFP after treatment of PCNs/ pENTR- *sh*BMP9.

Figure 3

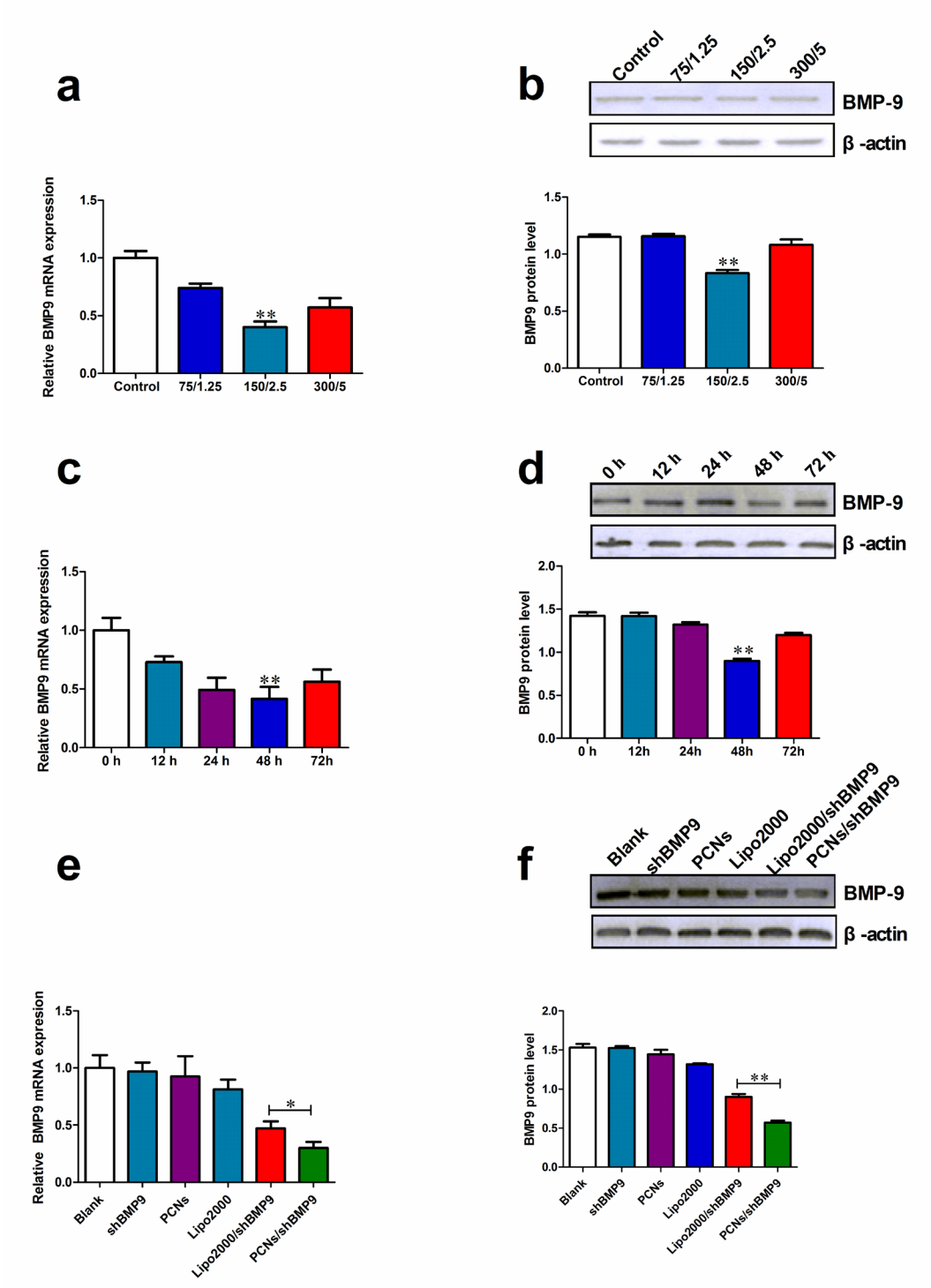

Figure 3. **Biological efficiency of pENTR-shBMP9 transfection using PCNs in *vitro***

The mRNA expression **(a)** and protein levels **(b)** of BMP9 in HepG2 cells transfected by PCNs/ pENTR-shBMP9 in various mass ratios. **(c)** The mRNA expression and protein levels

(d) of BMP9 in HepG2 cells transfected by PCNs/ pENTR- *sh*BMP9 in different times. **(e)** The mRNA expression and protein levels **(f)** of BMP9 in HepG2 cells transfected by pENTR-*sh*BMP9 mediated by PCNs or lipofectamine 2000. The data are shown as means ± SD and presented as the relative expression. **P* < 0.05, ***P* <0.01 *vs.* controls, 0-h or lipo2000/*sh*BMP9. PCNs/*sh*BMP9: PCNs/pENTR-*sh*BMP9; Lipo2000/ *sh*BMP9: pENTR-*sh*BMP9 is transfected by lipofectamine 2000

Figure 4

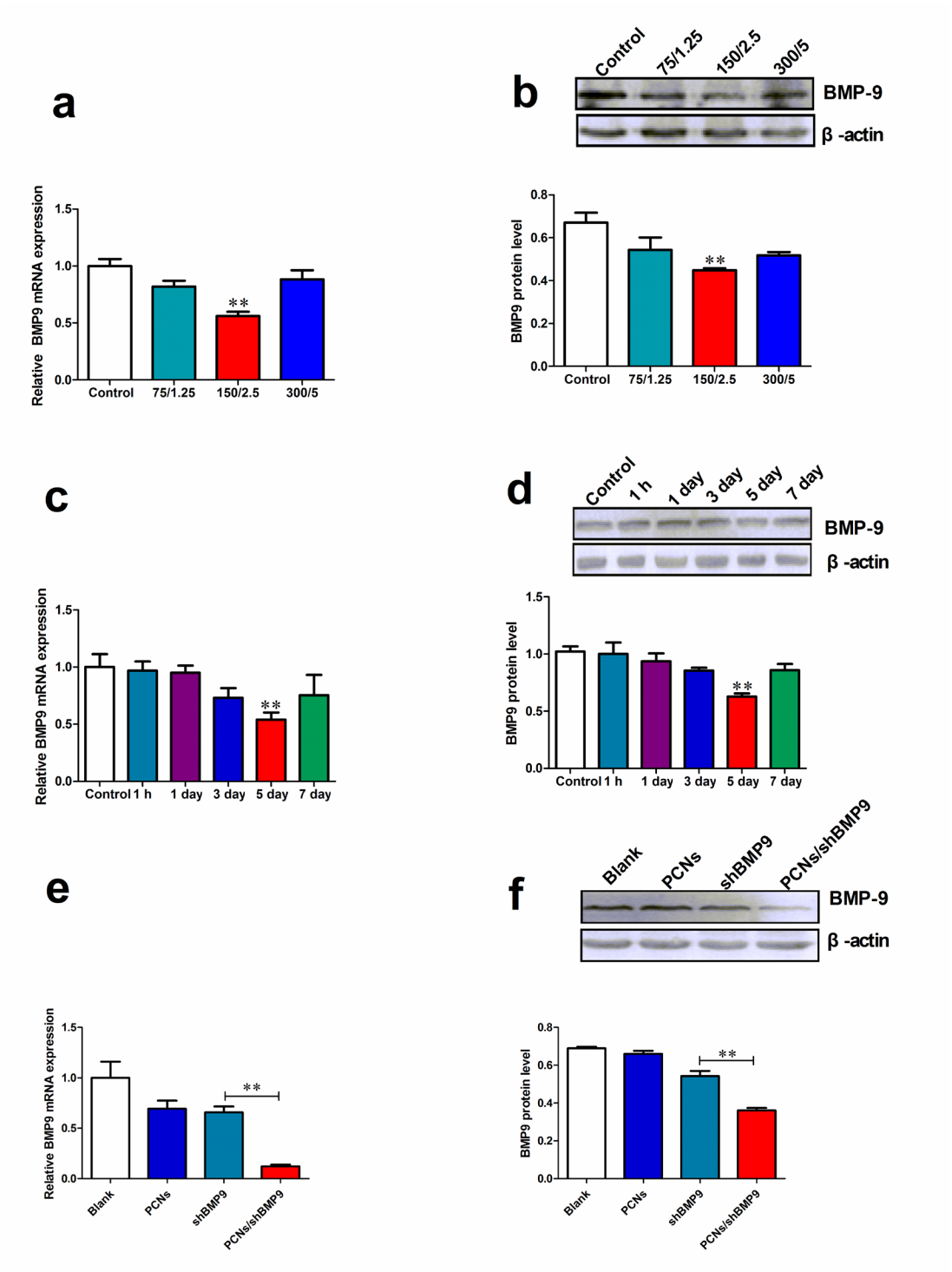

Figure 4 Biological efficiency of pENTR-shBMP9 transfection using PCNs in *vivo*.

(a-b) The mRNA expression **(a)** and protein levels **(b)** of BMP9 in the liver of C57BL/6J mice transfected by PCNs/pENTR-*sh*BMP9 in various mass ratios. **(c)** The mRNA expression

and protein levels **(d)** of BMP9 in HepG2 cells transfected by PCNs/ pENTR-shBMP9 in different times. **(e)** The mRNA expression and protein levels **(f)** of BMP9 in the liver of C57BL/6J mice transfected by PCNs/ pENTR-*sh*BMP9 (PCNs/ *sh*BMP9) or pENTR-*sh*BMP9 (*sh*BMP9). The data are shown as means ± SD and presented as the relative expression. **P* < 0.05, ***P* <0.01 *vs.* controls or *sh*BMP9.

Figure 5

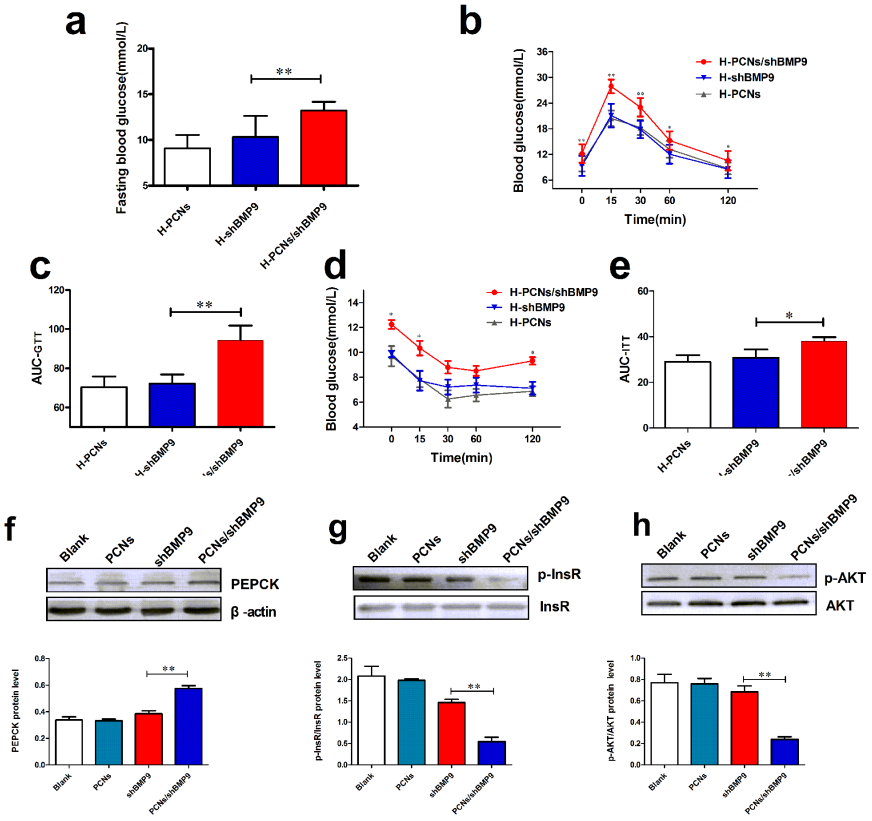

Figure 5 The effects of pENTR-*sh*BMP9 transfection using PCNs on blood glucose and insulin sensitivity in *vivo*. (a) Fasting blood glucose in different-treated mice. Plasma glucose levels **(b)** and AUC_{GTT} **(c)** in different-treated mice during GTT. Plasma glucose levels **(d)** and AUC_{ITT} **(e)** in different-treated mice during ITT. PCNs, PCNs-treated mice; **(f)** PEPCK protein levels in the liver of C57BL/6J mice transfected by PCNs/pENTR-*sh*BMP9 or pENTR-*sh*BMP9. The phosphorylation of InsR **(g)** and Akt **(h)** in the liver of C57BL/6J mice transfected by PCNs/pENTR-*sh*BMP9 or pENTR- *sh*BMP9. shBMP9, pENTR-*sh*BMP9-treated mice; PCNs/*sh*BMP9, PCNs/ pENTR-*sh*BMP9-treated mice; AUC_{GTT}, the area under the curve for glucose; AUC_{ITT}, the area under the curve for insulin. The data are shown as means ± SD and presented as the relative expression. **P* <0.05 or ***P* <0.01 *vs. sh*BMP9.